2010

# System Development for High Frequency Ultrasound-Guided Fluorescence Quantification of Skin Layers

Josiah D. Gruber

Akshat Paliwal

Venkataramanan Krishnaswamy
*Dartmouth College*

Hamid Ghadyani

# System development for high frequency ultrasound-guided fluorescence quantification of skin layers

**Josiah D. Gruber**
Dartmouth College
Thayer School of Engineering
8000 Cummings Hall
Hanover, New Hampshire 03755

**Akshat Paliwal**
Lerner Research Institute
Department of Biomedical Engineering
9500 Euclid Avenue
Cleveland, Ohio 44195

**Venkataramanan Krishnaswamy**
**Hamid Ghadyani**
**Michael Jermyn**
**Julie A. O'Hara**
**Scott C. Davis**
Dartmouth College
Thayer School of Engineering
8000 Cummings Hall
Hanover, New Hampshire 03755

**Joanna S. Kerley-Hamilton**
**Nicholas W. Shworak**
Dartmouth Medical School
Department of Medicine
1 Medical Center Drive
Lebanon, New Hampshire 03756

**Edward V. Maytin**
Lerner Research Institute
Department of Biomedical Engineering
9500 Euclid Avenue
Cleveland, Ohio 44195
and
Harvard Medical School
Massachusetts General Hospital
Wellman Center for Photomedicine
Boston, Massachusetts 20114

**Tayyaba Hasan**
Harvard Medical School
Massachusetts General Hospital
Wellman Center for Photomedicine
Boston, Massachusetts 20114

**Brian W. Pogue**
Thayer School of Engineering
Dartmouth College
Hanover, New Hampshire 03755
and
Massachusetts General Hospital
Wellman Center for Photomedicine
Boston, Massachusetts 20114

**Abstract.** A high frequency ultrasound-coupled fluorescence tomography system, primarily designed for imaging of protoporphyrin IX production in skin tumors *in vivo*, is demonstrated for the first time. The design couples fiber-based spectral sampling of the protoporphyrin IX fluorescence emission with high frequency ultrasound imaging, allowing thin-layer fluorescence intensities to be quantified. The system measurements are obtained by serial illumination of four linear source locations, with parallel detection at each of five interspersed detection locations, providing 20 overlapping measures of subsurface fluorescence from both superficial and deep locations in the ultrasound field. Tissue layers are defined from the segmented ultrasound images and diffusion theory used to estimate the fluorescence in these layers. The system calibration is presented with simulation and phantom validation of the system in multilayer regions. Pilot *in-vivo* data are also presented, showing recovery of subcutaneous tumor tissue values of protoporphyrin IX in a subcutaneous U251 tumor, which has less fluorescence than the skin.

[DOI: 10.1117/1.3374040]

Keywords: tomography; ultrasound-coupled fluorescence; protoporphyrin IX; skin tumors.

Paper 10038LR received Feb. 1, 2010; revised manuscript received Mar. 1, 2010; accepted for publication Mar. 2, 2010; published online Apr. 13, 2010.

## 1 Introduction

Skin cancer cells are known to produce a highly fluorescent porphyrin called protoporphyrin IX (PpIX), when aminolevulinic acid (ALA) is applied,[1–3] and its use is approved for photodynamic treatment of superficial forms of squamous cell carcinoma (SCC) and basal cell carcinoma (BCC). For thicker skin carcinomas, a major concern has been the inability to measure the amount of PpIX production that is occurring at deep tumor locations. Adjuvant methods to stimulate PpIX could work, such as differentiation therapy,[4] and better tools are needed to assess if enhanced PpIX production is obtained in individual subjects. The goal of the current study is to develop and test a system that can quantify PpIX concentrations in skin tumor tissue by directly measuring the signal emitted from the tissue surface, while simultaneously quantifying the tumor margin with high frequency ultrasound

Address all correspondence to: Brian Pogue, Dartmouth College, Hanover, New Hampshire 03755. Tel: 603-646-3861; Fax: 603-646-3856; E-mail: brian.w.pogue@dartmouth.edu

1083-3668/2010/15(2)/026028/5/$25.00 © 2010 SPIE

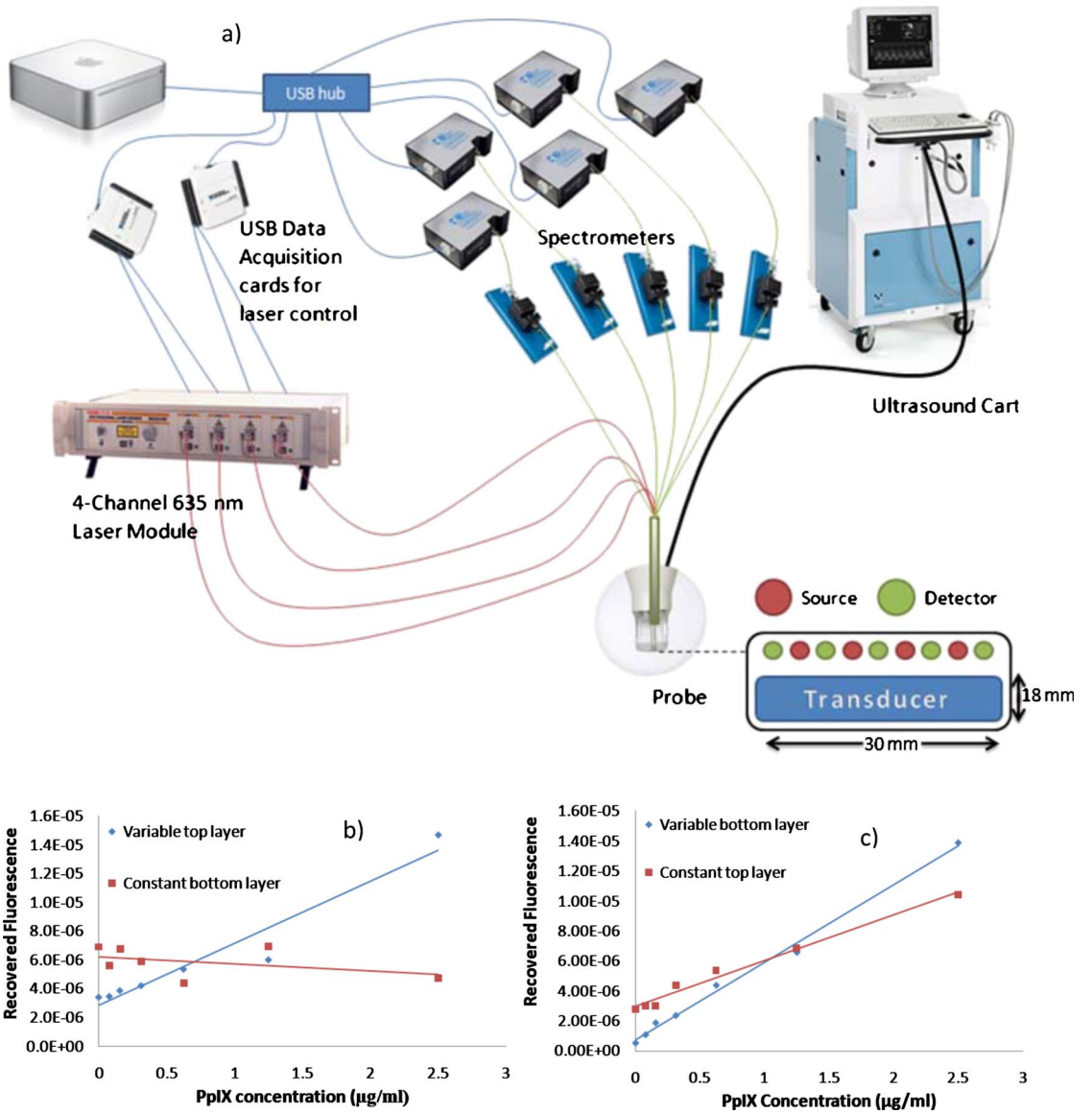


**Fig. 1** The system schematic is illustrated in (a) showing components and probe geometry, with data acquisition from five compact spectrometers. The recovered fluorescence values for the layers (b) with the top concentration varied and the bottom fixed at 0.625 $\mu$g/ml. In (c), the top layer was held constant and the bottom layer varied.

(HFUS). Preclinical development and testing of this device was the subject of this study, with full calibration, tissue phantom testing, and a pilot study in a preclinical model.

This approach to guide the interpretation of the fluorescence signal[5–7] is beneficial because subsurface tomography with light is quite challenging. Subsurface diffuse optical tomography without any additional imaging is known to be inaccurate[8,9] because of the ill-posed numerical inversion problem. High scatter and absorption attenuation contribute to a nonlinear relationship between detected signal and PpIX concentration. Image-guided fluorescence tomography[10] with HFUS should allow characterization of skin layers and tumor PpIX concentrations. Hybrid ultrasound/optical imaging was demonstrated by other researchers, most notably substantial developments in breast tumor imaging by Zhu et al.[11] In this work, the hardware and software[12] were designed for automated calibration and were tested in phantoms, along with an initial preclinical demonstration.

## 2 Materials and Methods

The system [schematic in Fig. 1(a)] has been assembled from low-cost, commercially available products and specifically designed to be as portable and modular as possible. There are four source and five detection channels that are automated through computer control. The lasers in the four-source module (ThorLabs, Newton, New Jersey, model MCSL635) are centered at 635-nm wavelength at 10-mW power. Laser outputs couple into 200-$\mu$m fibers, and intensities are electronically controlled from LabView controlled data acquisition (DAQ) cards (National Instruments, Austin, Texas, model USB 6009). All four sources were stable to within 0.5 to 4%

over a time period of 15 min, and repeatable to within 1 to 4% for successive system starts.

In detection, five compact USB-coupled spectrometers (Ocean Optics, Dunedin, Florida, model USB2000+) are used for each fiber, with a wavelength resolution of 0.37 nm and spectral bandwidth of 540 to 1210 nm. An inline filter holder (OceanOptics, model FHS-UV) with a 650-nm long pass filter (ThorLabs, FEL0650) is used to remove the 635-nm source signals while allowing passage of the PpIX fluorescence, peaked at 705-nm wavelength.

Source and detector fibers alternate linearly along the length of the tissue contact probe [Fig 1(a)] just adjacent to the ultrasound probe. The holder protects the fibers while also immobilizing them above gradient index (GRIN) lenses (Newport Corporation, Irvine, California, model LGI630-6), that focus them 5 mm below the probe surface, matching the height of the clear gel coupling the ultrasound system to the tissue surface.

Ultrasound imaging was conducted with a Vevo 770 (VisualSonics, Toronto, Ontario) using either an RMV-708 (82.5-MHz maximum frequency; 30-$\mu$m axial and 70-$\mu$m lateral resolution with 10.8-mm field of view) or a RMV-704 (60-MHz maximum frequency; 40-$\mu$m axial and 80-$\mu$m lateral resolution with 14.6-mm field of view) scan head. For *in-vivo* imaging, mice were anesthetized with about 2.5% isoflurane initially and reduced to 1.5% during imaging, and were positioned on a thermoregulated platform. The scan head/optical detector complex was held in place during imaging acquisition. An ultrasound snapshot was taken in the tumor plane, and then the sample is moved until it is in the plane of the optical sources and detectors.

The software acquires background levels and sequenced each of the four lasers while capturing all five detector spectra. The signal in the spectrum that was not part of the 705-nm PpIX peak was due to broadening of the 635-nm laser source and autofluorescence. The data are automatically calibrated for individual response, and autofluroescence is removed. Simulations were done to validate the accuracy of our system's measurements using the finite element-based NIRFast Matlab software.[8]

System validation was performed using heterogeneous tissue phantoms using 1% Intralipid™ for scattering and 0.002% India ink for absorption,[13] with 5% Tween-20 to monomerize the PpIX. This was mixed with 1% agarose (Sigma Aldrich, Saint Louis, Missouri) in water heated to the boiling point, and then cooled at 4 °C for 15 min to create solid fluorescent phantoms. Imaging of two-layer gelatin phantoms was performed with the PpIX concentration of the bottom 10-mm layer fixed at 0.625 $\mu$g/mL, and the top 1 to 2-mm layer varied from 0 to 2.5 $\mu$g/ml. The reverse case was also imaged—holding the top layer constant at 0.625 $\mu$g/ml and varying the bottom layer from 0 to 2.5 $\mu$g/ml.

## 3 Results

The results of all two-layer phantom experiments are displayed in Figs. 1(b) and 1(c). Interestingly, the recovery of fluorescence yield is always perfectly accurate in the layer that has the higher fluorescence. Yet in both the lower and upper layers, when the fluorescence is lower than the opposite layer, the recovery is not fully accurate. This figure shows the experimental validation of the system in a controlled manner. As might be expected, when the fluorescence is very low, there is a higher fluorescence recovered, because the signal from the opposite layer is presumably causing some overestimation of the lower region.

Figure 2 demonstrates the ability of the system to give reasonable reconstructed images for three-layer gelatin phantoms. For these experiments, a thin layer of gelatin with PpIX was placed over a bump of gelatin with a different concentration of PpIX. The bump sizes were $15\times15\times3$ mm. The bottom layer consisted of gelatin with no PpIX fluorescence. This accurately simulated the situation seen when imaging subcutaneous tumors in mice. The top layers of the image were segmented, and a Matlab routine created the finite element meshes in Fig. 2.[14] Each region of the mesh was assumed to be homogeneous in fitting for fluorescence in the tissue types. Figure 2(a) shows recovery of a simulated tumor region with higher fluorescence than the skin, and Fig. 2(b) shows recovery when the simulated tumor region was lower than the skin.

All procedures using animals were approved by the Institutional Animal Care and Use Committee. The rat U251 gliosarcoma cells were implanted in phosphate buffered saline (PBS) at $2\times10^7$ cells/ml with 50 $\mu$L into the nude mice skin and grown 7 to 14 days for a 3- to 7-mm-diam tumor. Tumors were imaged after ALA injection 2 h prior. Figure 2(i) shows a typical result for a subcutaneous tumor in a mouse. Mouse skin is highly fluorescent compared to the tumor, as expected. These results were verified with *ex-vivo* fluorescence scanning of the tissues (GE Healthcare Typhoon) to validate the images. These images indicate that the skin contains nearly four times the fluorescence found in U251 tumors [Fig. 2(j)]. The shape of the tumor matches exactly the shape of the fluorescent overlay, since the ultrasound image was used to guide the solution.

## 4 Discussion

Accurate quantification of PpIX production in skin tumors remains an ongoing challenge. PpIX production and treatment efficacy are unclear for deeper tumors, yet methods to enhance production are available. High-frequency ultrasound provides a clear structural image that allows us to combine anatomical information with fluorescence data for reconstruction algorithms.

In creation of an ultrasound-guided fluorescence recovery system, the system integration was straightforward and modular, and phantom testing provided a way to validate the system. The problem of subsurface tomography is known to be confounded when there is an upper layer that is significantly more fluorescent than the lower layer. Intuitively, it is possible to realize that as the upper layer fluorescence level increases, eventually the lower layer signal will be lost in the noise of the detection system as the upper layer dominates the detected signal. As such, there will always be a lower limit, below which the lower fluorescence layer cannot be effectively quantified or even detected with decreasing depth or with decreasing contrast. In the experimental case here, when the tumors have lower PpIX production than the overlying skin, and as shown in Fig. 2, the more fluorescent layer of the skin tends to dominate the reconstruction algorithm. The simulations and phantom data indicate that the system has a suffi-

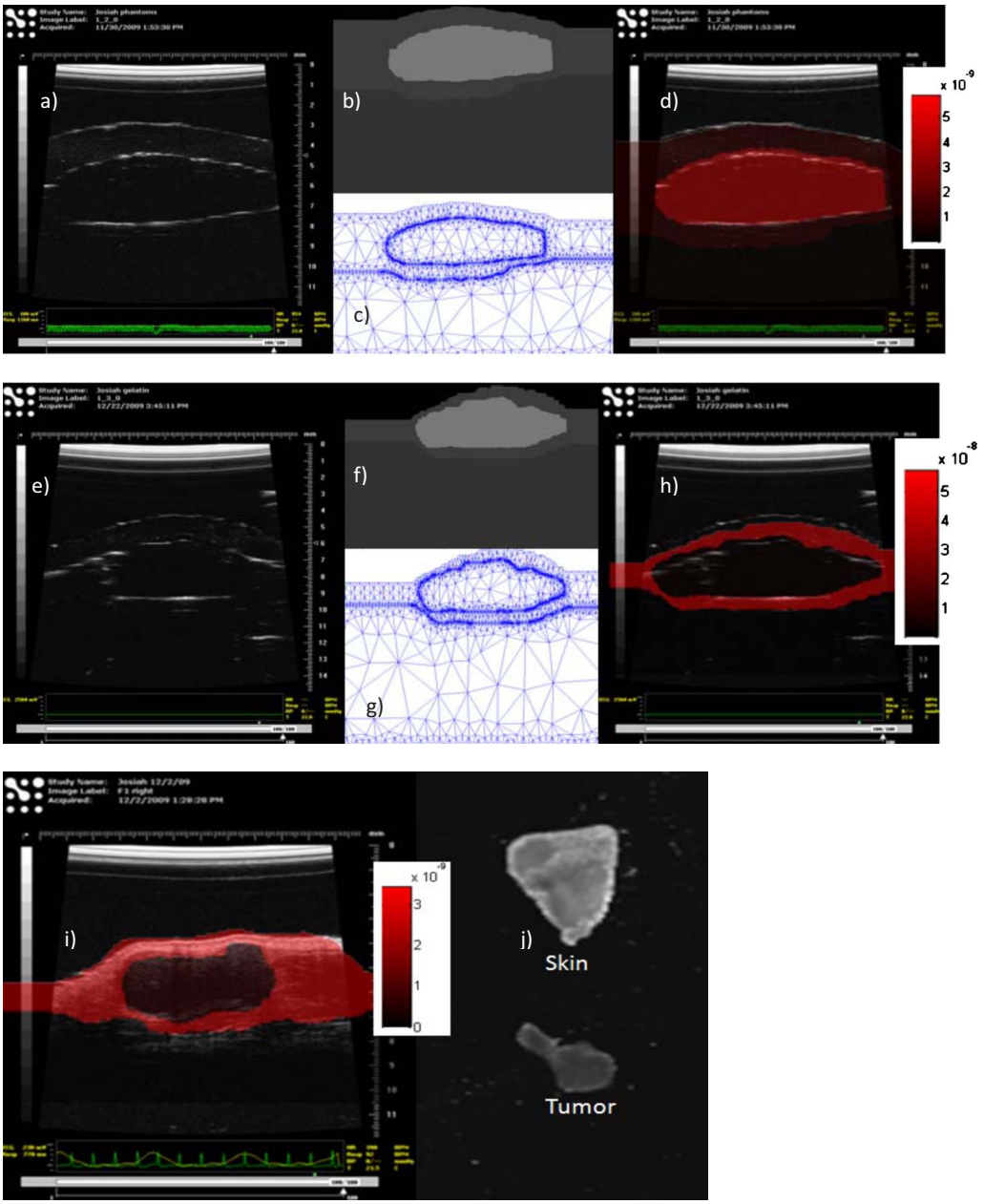


**Fig. 2** The images of complex gelatin phantoms are shown with two different PPIX concentrations with: (a) HFUS image of layers; (b) segmented image from the HFUS image; (c) the mesh created; and (d) reconstructed fluorescence map overlaid on top of the HFUS image from (a). In the second phantom, (e) the HFUS image showing the layers; (f) the segmented image; (g) the mesh created; and (h) the reconstructed fluorescence map overlaid on the HFUS image from (e). Images of a subcutaneous U251 tumor are also shown with (i) a reconstructed fluorescence map overlaid on the HFUS and (j) the *ex-vivo* fluorescence images of skin and tumor.

ciently good signal-to-noise region to recover tumor fluorescence images down to several millimeters depth, but the lower layer is most inaccurate due to confounding information in the upper layer. The image segmentation still must be user-guided to avoid errors from the speckle and noise in the ultrasound images, but the segmentation process of region growing works well with just seconds of user guidance.

## 5 Conclusions

A system development study creating the first high-frequency ultrasound-guided fluorescence tomography system is initiated for imaging skin tumors. Simulations and phantoms studies show that the system works well. Phantom results demonstrate the ability to determine fluorescence in multilayer situations mimicking skin tumors, and initial *in-vivo* imaging is promising. Preclinical studies are ongoing to analyze the system performance with various shapes, sizes, depths, PpIX concentrations, and to improve the recovered contrast values.

### *Acknowledgments*

The authors are extremely grateful to Subhadra Srinivasan, Hamid Dehghani, and Keith Paulsen for productive discussions about the algorithm development. This work has been funded by NIH Program Project P01CA84203.

## References


1. J. Kennedy, "Endogenous protoporphyrin IX, a clinically useful photosensitizer for photodynamic therapy," *J. Photochem. Photobiol.* **14**(4), 275–292 (1992).
2. Z. Hua, S. L. Gibson, T. H. Foster, and R. Hilf, "Effectiveness of {delta}-aminolevulinic acid-induced protoporphyrin as a photosensitizer for photodynamic therapy in vivo," *Cancer Res.* **55**(8), 1723–1731 (1995).
3. Z. Malik, G. Kostenich, L. Roitman, B. Ehrenberg, and A. Orenstein, "Topical application of 5-aminolevulinic acid, DMSO and EDTA: protoporphyrin IX accumulation in skin and tumours of mice," *J. Photochem. Photobiol., B* **28**(3), 213–218 (1995).
4. B. Ortel, N. Chen, J. Brissette, G. P. Dotto, E. Maytin, and T. Hasan, "Differentiation-specific increase in ALA-induced protoporphyrin IX accumulation in primary mouse keratinocytes," *Br. J. Cancer* **77**(11), 1744–1751 (1998).
5. Q. Zhu, N. G. Chen, D. Piao, P. Guo, and X. Ding, "Design of near-infrared imaging probe with the assistance of ultrasound localization," *Appl. Opt.* **40**(19), 3288–3303 (2001).
6. Q. Zhu, S. H. Kurtzma, P. Hegde, S. Tannenbaum, M. Kane, M. Huang, N. G. Chen, B. Jagjivan, and K. Zarfos, "Utilizing optical tomography with ultrasound localization to image heterogeneous hemoglobin distribution in large breast cancers," *Neoplasia* **7**(3), 263–270 (2005).
7. C. M. Carpenter, B. W. Pogue, S. Jiang, H. Dehghani, X. Wang, K. D. Paulsen, W. A. Wells, J. Forero, C. Kogel, J. B. Weaver, S. P. Poplack, and P. A. Kaufman, "Image-guided optical spectroscopy provides molecular-specific information in vivo: MRI-guided spectroscopy of breast cancer hemoglobin, water, and scatterer size," *Opt. Lett.* **32**(8), 933–935 (2007).
8. D. S. Kepshire, S. C. Davis, H. Dehghani, K. D. Paulsen, and B. W. Pogue, "Subsurface diffuse optical tomography can localize absorber and fluorescent objects but recovered image sensitivity is nonlinear with depth," *Appl. Opt.* **46**(10), 1669–1678 (2007).
9. D. Kepshire, S. C. Davis, H. Dehghani, K. D. Paulsen, and B. W. Pogue, "Fluorescence tomography characterization for sub-surface imaging with protoporphyrin IX," *Opt. Express* **16**(12), 8581–8593 (2008).
10. S. C. Davis, H. Dehghani, J. Wang, S. Jiang, B. W. Pogue, and K. D. Paulsen, "Image guided diffuse optical fluorescence tomography implemented with Laplacian-type regularization," *Opt. Express* **15**(7), 4066–4082 (2007).
11. Q. Zhu, T. Durduran, V. Ntziachristos, M. Holboke, and A. G. Yodh, "Imager that combines near-infrared diffusive light and ultrasound," *Opt. Lett.* **24**(15), 1050–1052 (1999).
12. H. Dehghani, M. E. Eames, P. K. Yalavarthy, S. C. Davis, S. Srinivasan, C. M. Carpenter, B. W. Pogue, and K. D. Paulsen, "Near infrared optical tomography using NIRFAST: algorithm for numerical model and image reconstruction," *Commun. Numer. Methods Eng.* (published online) (2008).
13. B. W. Pogue and M. S. Patterson, "Review of tissue simulating phantoms for optical spectroscopy, imaging and dosimetry," *J. Biomed. Opt.* **11**(4), 041102 (2006).
14. H. Ghadyani, J. Sullivan, and Z. Wu, "Boundary recovery for Delaunay tetrahedral meshes using local topological transformations," *Finite Elem. Anal. Design* **46**(1–2), 74–83 (2010).